DOI: 10.3901/CJME.2014.0912.150, available online at www.cjmenet.com; www.cjmenet.com.cn

Influence of Tire Dynamics on Slip Ratio Estimation of Independent Driving Wheel System

LI Jianqiu, SONG Ziyou, WEI Yintao, and OUYANG Minggao*

State Key Laboratory of Automotive Safety and Energy, Tsinghua University, Beijing 100084, China

Received June 20, 2013; revised July 2, 2014; accepted September 12, 2014

Abstract: The independent driving wheel system, which is composed of in-wheel permanent magnet synchronous motor(I-PMSM) and tire, is more convenient to estimate the slip ratio because the rotary speed of the rotor can be accurately measured. However, the ring speed of the tire ring doesn't equal to the rotor speed considering the tire deformation. For this reason, a deformable tire and a detailed I-PMSM are modeled by using Matlab/Simulink. Moreover, the tire/road contact interface(a slippery road) is accurately described by the non-linear relaxation length-based model and the Magic Formula pragmatic model. Based on the relatively accurate model, the error of slip ratio estimated by the rotor rotary speed is analyzed in both time and frequency domains when a quarter car is started by the I-PMSM with a definite target torque input curve. In addition, the natural frequencies(NFs) of the driving wheel system with variable parameters are illustrated to present the relationship between the slip ratio estimation error and the NF. According to this relationship, a low-pass filter, whose cut-off frequency corresponds to the NF, is proposed to eliminate the error in the estimated slip ratio. The analysis, concerning the effect of the driving wheel parameters and road conditions on slip ratio estimation, shows that the peak estimation error can be reduced up to 75% when the LPF is adopted. The robustness and effectiveness of the LPF are therefore validated. This paper builds up the deformable tire model and the detailed I-PMSM models, and analyzes the effect of the driving wheel parameters and road conditions on slip ratio estimation.

Keywords: electric vehicle (EV), driving wheel system, tire dynamics, slip ratio estimation, characteristic frequency, low-pass filter (LPF)

1 Introduction

It is estimated that current global petroleum resources could be used up within 50 years if they are consumed at present consumption rates[1]. The electric vehicle(EV), which is receiving great attention, is an effective solution for energy and environmental problems. EV's advantages over internal combustion engine vehicle can be summarized as follows[2–3].

(1) The torque response of electric motors is 10–100 times faster than that of engines.

(2) All wheels can be controlled independently by adopting small high-power in-wheel motors.

(3) The output torque of an electric motor can be measured accurately from the motor current.

The in-wheel permanent-magnet synchronous motor (I-PMSM) is widely used in engineering applications because of its high torque, high power density, high efficiency, and so on[4]. With regard to the PMSM control, the field-oriented control (FOC) algorithm is used in this paper thanks to its legible logic and good performance on ripple-free torque production[5–8].

Many traction control methods for anti-skid on slippery surface have been proposed based on the flexible dynamic control effect of EVs[3, 9–12]. In these control methods, slip ratio is a relevant state variable[3, 11–12] even a control objective[9–10]. Thus the slip ratio estimation is of vital importance to improve the vehicle performance. Several effective slip ratio estimation methods, using a slip ratio estimator or a slip ratio observer, have been proposed to estimate the slip ratio and vehicle velocity[13–14]. However, the rotor rotary speed is used in all estimation methods to calculate slip ratio without any compensation. It means that the tire deformation, which will cause the difference between the rotor speed and the tire ring speed, is not considered. The error introduced by the tire torsional dynamics may significantly affect the driving wheel performance under aggressive driving/braking events[15–17]. From this standpoint, a model combining the tangential tread-deflection model and the average Lumped Parameter LuGre friction model[18–19] is used in this study. Furthermore, the tire/road contact interface(a uniform low-μ surface) is accurately described by the non-linear relaxation length-based model[20] and the Magic Formula pragmatic model[21]. The accurate tire model will ensure the

* Corresponding author. E-mail: ouymg@tsinghua.edu.cn

Supported by National Natural Science Foundation of China (Grant Nos. 51275264, 51275265), and National Hi-tech Research and Development Program of China (Grant No. 2012DFA81190)

accuracy of real slip ratio estimation derived from the ring speed and the vehicle speed.

Based on the near-precise driving wheel model, a quarter in-wheel-motored car with typical parameters is modeled in this paper to present the slip ratio estimation error under the starting/accelerating condition in time and frequency domains. The relationship between the characteristic frequency(CF) of the driving wheel system and the estimation error in slip ratio is shown distinctly in frequency domain. In consequence, a low pass filter(LPF) whose cut-off frequency corresponds to the characteristic frequency of driving wheel system is proposed in this paper to eliminate the slip ratio estimation error.

Finally, the analysis examining the sensitivity of the dynamic tire and I-PMSM parameters(rotor/hub inertia, ring inertia, sidewalls torsional stiffness and damping coefficient) on the slip ratio estimation result is given. The simulation results verify the robustness and effectiveness of the proposed LPF. As a result, it can be used in practical applications to estimate the slip ratio accurately.

This paper is organized as follows. Firstly, the quarter in-wheel-motored car is modeled. Secondly, the error in the slip ratio, which is estimated by the rotor speed, is illustrated. Furthermore, the relationship between the slip ratio estimation error and the CF is analyzed in frequency domain. Then, the LPF is designed to eliminate the slip ratio estimation error. Thirdly, the driving wheel parameter sensitivity is analyzed, and the robustness and effectiveness of the proposed LPF are verified. At last, several conclusions are drawn.

2 Quarter In-wheel-motored Vehicle Modeling

2.1 I-PMSM modeling[22–25]

The following assumptions are made before establishing the mathematical model of PMSM.

(1) Neglects the saturation of the electric motor ferrite core.

(2) Neglects turbulent flow and hysteresis loss in electric motor.

(3) The current in electric motor is symmetrical three-phase sinusoidal current.

In FOC algorithm, both the three-phase stator *A*-*B*-*C* coordinate system and the two-phase stator α-β coordinate system are the static coordinate system. While the *d*-*q* coordinate system is revolving, the transforms between these three coordinates are given:

$$\begin{pmatrix} i_\alpha \\ i_\beta \end{pmatrix} = \sqrt{\frac{2}{3}} \begin{pmatrix} 1 & -\frac{1}{2} & -\frac{1}{2} \\ 0 & -\frac{\sqrt{3}}{2} & \frac{\sqrt{3}}{2} \end{pmatrix} \begin{pmatrix} i_a \\ i_b \\ i_c \end{pmatrix}, \tag{1}$$

$$\begin{pmatrix} i_d \\ i_q \end{pmatrix} = \begin{pmatrix} \cos\theta & \sin\theta \\ -\sin\theta & \cos\theta \end{pmatrix} \begin{pmatrix} i_\alpha \\ i_\beta \end{pmatrix}, \tag{2}$$

where i_a, i_b, i_c—*A*-, *B*- and *C*-axis currents,
i_d, i_q—*d*- and *q*-axis currents,
i_α, i_β—α- and β-axis currents.

The torque of the PMSM is determined by the i_d and i_q:

$$T_e = P_n \psi_a i_q + P_n (L_d - L_q) i_d i_q , \tag{3}$$

where L_d, L_q—*d*- and *q*-axis inductances,
Ψ_α—Permanent magnet flux-linkage,
T_e—Electromagnetic torque of motor,
P_n—Number of pole pairs.

In this study, a surface-mounted PMSM in which L_d equals to L_q is used so the torque Eq. (3) is simplified:

$$T_e = P_n \psi_a i_q = K i_q , \tag{4}$$

As shown in Fig. 1, the FOC algorithm has been widely used in PMSM torque control. The basic parameters of the I-PMSM used in this study are shown in Table 1.

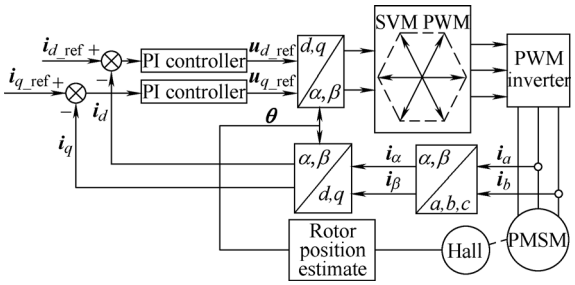

Fig. 1. Schematic diagram of FOC control strategy

Table 1. Parameters of the simulation I-PMSM

Parameter	Value
Pole pairs P_n	4
d-, *q*-axis inductance L_d, L_q/mH	8.5
Stator phase resistance R/Ω	0.2
Torque constant ψ_a/(N • m • A^{-1})	6.037 5
Rotary inertia J_{rotor}/(kg • m^2)	0.3

2.2 Driving wheel modeling

The model of driving wheel system is comprised of the I-PMSM model and the two-inertia tire model. The tire sidewall's torsional stiffness and damping coefficient are denoted K_r and C_r, respectively. The schematic for this model is shown in Fig. 2[16].

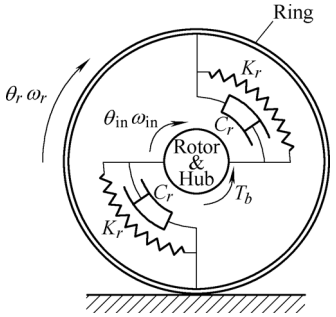

Fig. 2. Driving wheel dynamics model

In this paper, the tire deformation is not neglected in tire dynamic analysis. Focusing on the I-PMSM/hub and ring/ground interactions, the equations describing the driving wheel system reduce to the following:

$$J_{\text{in}}\ddot{\theta}_{\text{in}} = T_e - K_r(\theta_{\text{in}} - \theta_{\text{r}}) - C_r(\dot{\theta}_{\text{in}} - \dot{\theta}_{\text{r}}), \tag{5}$$

$$J_{\text{Ring}}\ddot{\theta}_{\text{r}} = K_r(\theta_{\text{in}} - \theta_{\text{r}}) + C_r(\dot{\theta}_{\text{in}} - \dot{\theta}_{\text{r}}) - F_x r, \tag{6}$$

$$J_{\text{in}} = J_{\text{Hub}} + J_{\text{rotor}}. \tag{7}$$

where θ_{in}, θ_{r}—Rotor/hub and ring angular position,
$\dot{\theta}_{\text{in}}$, $\dot{\theta}_{\text{r}}$—Rotor/hub and ring angular speed,
$\ddot{\theta}_{\text{in}}$, $\ddot{\theta}_{\text{r}}$—Rotor/hub and ring angular acceleration,
J_{Hub}, J_{Rotor}, J_{Ring}—Hub, rotor and ring inertia,
J_{in}—Inner hub inertia.

The tire/road contact interface(a uniform low-μ surface) is described by the Magic Formula pragmatic model and non-linear relaxation length-based model. The Magic Formula pragmatic model indicates the relationship between slip ratio s_x and steady longitudinal force F_x^{S}:

$$s_x = \frac{\dot{\theta}_{\text{r}} r - V}{V}, \tag{8}$$

$$F_x^{\text{S}} = D\sin[C\arctan(Bs_x - E(Bs_x - \arctan Bs_x))], \tag{9}$$

where r—Effective rolling radius of tire,
V—Vehicle speed,
D—Peak factor,
B—Stiffness factor,
E—Curvature factor.

A typical tire is chosen in this study and the parameters B, C, D, and E are estimated by experiments[21] which are shown below(a slippery road):

$$C = 1.685,\ E = 0.344, \tag{10}$$

$$D = \frac{1}{2}\frac{4840}{(1+V/16.67)}, \tag{11}$$

$$B = \frac{86\,040}{[8155.4/(1+V/16.67)+0.1]}. \tag{12}$$

Measurements show that the dynamic reaction of tire force to disturbances can be approximated quite well by the first order system. The non-linear relaxation length-based model is used to figure out the dynamic longitudinal force F_x^{D} derived from the steady longitudinal force:

$$\tau\dot{F}_x^{\text{D}} + F_x^{\text{D}} = F_x^{\text{S}}, \tag{13}$$

The time constant τ can be derived from the so-called relaxation length r_x:

$$\tau = \frac{r_x}{r\dot{\theta}_{\text{r}}}, \tag{14}$$

The relaxation length is the function of the slip ratio s_x and the wheel load F_z but the detailed function is too complex to be used in the simulation. Therefore a look-up table indicating the computed relaxation changed with various F_z and s is necessary[16], as presented in Fig. 3.

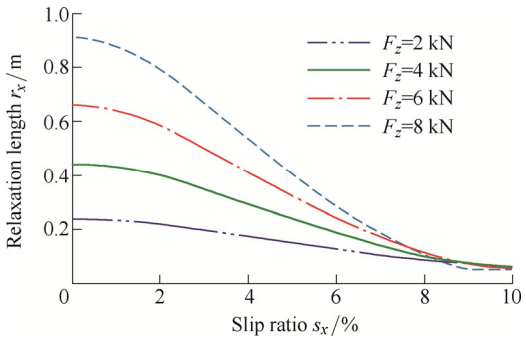

Fig. 3. Computed relaxation length characteristics

Based on the model illustrated above, a quarter car model is established:

$$F_f = \frac{M}{4}(0.007\,6 + 0.000\,2V) + 0.25\frac{C_D A V^2}{5.875}, \tag{15}$$

$$\dot{V} = \frac{F_x^{\text{D}} - F_f}{M/4}, \tag{16}$$

where M—Vehicle mass,
C_D—Drag coefficient,
A—Wind area,
F_f—Drag force.

The basic parameters of the quarter car are listed in Table 2.

Table 2. Parameters of the quarter car

Parameter	Value
Hub inertia J_{Hub}/(kg • m^2)	0.7
Ring inertia J_{Ring}/(kg • m^2)	0.5
Torsional stiffness K_r/(N • m • rad^{-1})	19 438
Damping coefficient C_r/(N • m • s • rad^{-1})	4
Effective rolling radius r/m	0.313
Vehicle mass M/kg	1600
C_DA/m^2	3.76

3 Slip Ratio Estimation Error

Considering the tire deformation, the slip ratio estimated by the rotor speed must contain some error especially under the fluctuating operation conditions, such as acceleration and deceleration. The error is caused by the difference

between the rotor and the ring speeds. The following simulation condition is that the quarter car is started with a changing torque target input(from 30 N • m to 280 N • m at 3 s), which is shown in Fig. 4, on a flat and low-μ road (μ=0.5). The initial vehicle speed is set to 0.01 m/s to amplify the error in estimated slip ratio (ESR). The speed difference between rotor and ring($\dot{\theta}_{\text{in}}-\dot{\theta}_{\text{r}}$) under the starting condition is shown in Fig. 5.

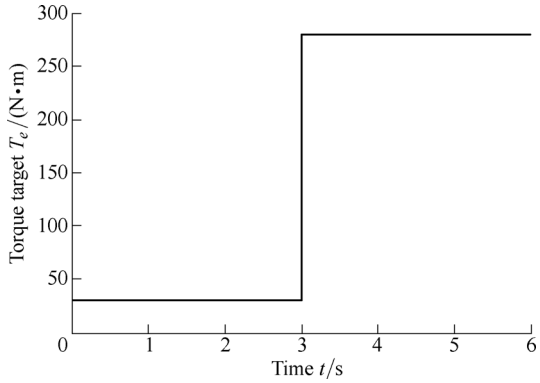

Fig. 4. Target torque of I-PMSM

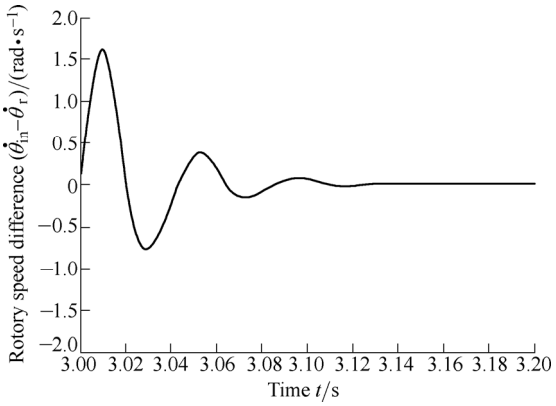

Fig. 5. Speed difference between rotor and ring

The vibration of the speed difference leads to a definite error in the slip ratio estimation. In order to present this error more clearly, the simulation result is given both in the time and the frequency domains as Fig. 6 and Fig. 7 shown.

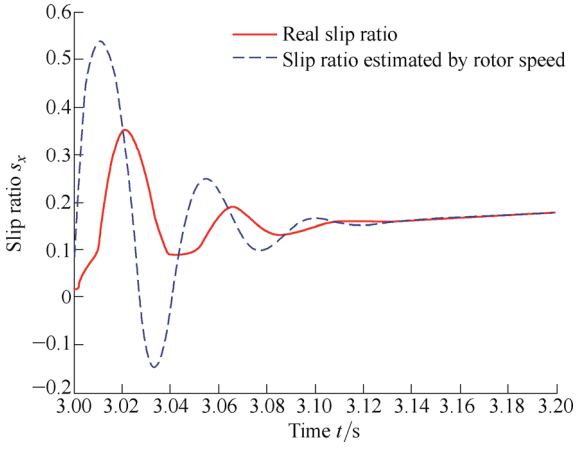

Fig. 6. Error in slip ratio estimated by rotor speed

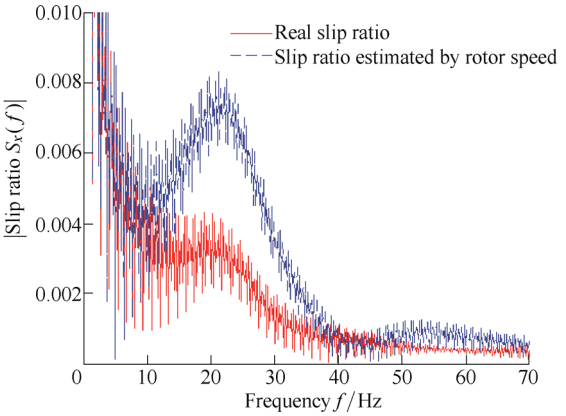

Fig. 7. FFT analysis of the slip ratio estimation error

The estimated slip ratio oscillates when the vehicle is started, then converge to the real slip ratio slowly. Fig. 6 shows the simulation result from 0.8 s to 1.6 s. In order to analyze the noise in the ESR more distinctly, a FFT comparison analysis between the real slip ratio(RSR) and the ESR is shown in Fig. 7, indicating that the centralized noise appears at about 23 Hz in comparison with the real slip ratio.

Based on the FFT analysis, a LPF is easy to be considered as a solution to eliminate the noise. The cut-off frequency of the LPF should be chosen according to the noise frequency, which is related to the natural frequency (NF) of the deformable tire. Before the design, the state-space model of the driving wheel system is analyzed.

Define

$$\boldsymbol{\theta}=(\theta_{\text{in}}\quad\theta_{\text{r}}\quad\dot{\theta}_{\text{in}}\quad\dot{\theta}_{\text{r}})^{\text{T}},\tag{17}$$

the state equations are derived from Eqs. (5) and (6):

$$\dot{\boldsymbol{\theta}}=\boldsymbol{A}\bullet\boldsymbol{\theta}+\boldsymbol{B}\bullet\boldsymbol{R},\tag{18}$$

$$\boldsymbol{A}=\begin{pmatrix}0 & 0 & 1 & 0\\ 0 & 0 & 0 & 1\\ -\dfrac{K_r}{J_{\text{in}}} & \dfrac{K_r}{J_{\text{in}}} & -\dfrac{C_r}{J_{\text{in}}} & \dfrac{C_r}{J_{\text{in}}}\\ \dfrac{K_r}{J_{\text{Ring}}} & -\dfrac{K_r}{J_{\text{Ring}}} & \dfrac{C_r}{J_{\text{Ring}}} & -\dfrac{C_r}{J_{\text{Ring}}}\end{pmatrix},\tag{19}$$

$$\boldsymbol{B}=\begin{pmatrix}0 & 0 & \dfrac{1}{J_{\text{in}}} & 0\\ 0 & 0 & 0 & -\dfrac{r}{J_{\text{Ring}}}\end{pmatrix}^{\text{T}},\tag{20}$$

$$\boldsymbol{R}=(T_e\quad F_x)^{\text{T}},\tag{21}$$

where $\boldsymbol{A}$ is state matrix, $\boldsymbol{B}$ is the input matrix, and $\boldsymbol{R}$ is the system input. Pole analysis of this system is given as follows:

$$|s \cdot \boldsymbol{I} - \boldsymbol{A}| = 0\,, \tag{22}$$

$$\begin{vmatrix} s & 0 & -1 & 0 \\ 0 & s & 0 & -1 \\ \dfrac{K_r}{J_{\text{in}}} & -\dfrac{K_r}{J_{\text{in}}} & s+\dfrac{C_r}{J_{\text{in}}} & -\dfrac{C_r}{J_{\text{in}}} \\ -\dfrac{K_r}{J_{\text{Ring}}} & \dfrac{K_r}{J_{\text{Ring}}} & -\dfrac{C_r}{J_{\text{Ring}}} & s+\dfrac{C_r}{J_{\text{Ring}}} \end{vmatrix} = 0\,, \tag{23}$$

$$s^4 + \left(\frac{C_r}{J_{\text{Ring}}} + \frac{K_r}{J_{\text{in}}}\right)s^3 + \left(\frac{K_r}{J_{\text{Ring}}} + \frac{C_r}{J_{\text{in}}}\right)s^2 = 0. \tag{24}$$

The pole points are obtained through Eq. (24):

$$\begin{cases} s_{1,2} = 0 \\ s_{3,4} = -\dfrac{C_r}{2J_{\text{in}}} - \dfrac{C_r}{J_{\text{Ring}}} \pm \\ \quad \sqrt{\left(\dfrac{C_r}{J_{\text{in}}}\right)^2 + \dfrac{2C_r^2}{J_{\text{in}}J_{\text{Ring}}} + \left(\dfrac{C_r}{J_{\text{Ring}}}\right)^2 - \dfrac{4K_r}{J_{\text{in}}} - \dfrac{4K_r}{J_{\text{Ring}}}} \Big/ 2. \end{cases} \tag{25}$$

Under normal conditions, C_r is much less than K_r. So the NF f_n is simplified as below:

$$f_n = \frac{\sqrt{\dfrac{K_r}{J_{\text{in}}} + \dfrac{K_r}{J_{\text{Ring}}}}}{\pi}. \tag{26}$$

In order to seek the relationship between f_n and the noise in ESR, different driving wheel systems with different parameters should be taken into consideration. The details of these five different driving wheels are presented in Table 3.

Table 3. Parameters of different driving wheels

Parameter	No. 1	No. 2	No. 3	No. 4	No. 5
Inner inertia J_{in}/(kg • m^2)	1	1	1	1	0.5
Ring inertia J_{Ring}/(kg • m^2)	0.5	0.5	0.5	0.5	0.25
Torsional stiffness K_r/(N • m • rad^{-1})	4859.5	9719	19 438	38 876	9719
Damping coefficient C_r/(N • m • s • rad^{-1})	4	4	4	4	4
Natural frequency f_n/Hz	19.21	27.18	38.43	54.35	38.43

The FFT analysis result is shown in Fig. 8 which indicates that frequency of the noise in ESR is proportional to the NF f_n, although they are not equal. Furthermore, the error magnitude of ESR decreases with the K_r increases (the tire tends to be rigid).

Before designing the LPF, define

$$f_{\text{cut}} = \frac{f_n}{N_0}, \tag{27}$$

where f_{cut}—Cut-off frequency of the LPF,
N_0—Proportional constant.

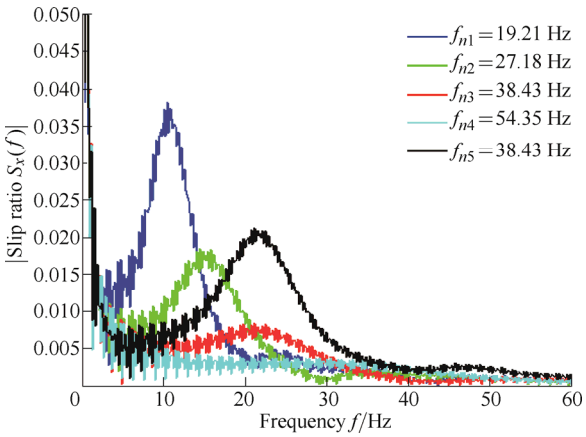

Fig. 8. FFT analysis of slip ratio estimation with various system natural frequencies

The problem is transferred to how to decide the parameter N_0. Based on the driving wheel system with typical parameters, Fig. 9 gives the simulation results of different LPF. Significant differences among the filtered ESRs when the LPF is adopted can be observed. It is obvious that the filtered ESR converges to the RSR most promptly when N_0 is 4. This conclusion is hard to deduce because the tire/road contact relational expression is highly non-linear. Furthermore, this conclusion will be verified in the next section.

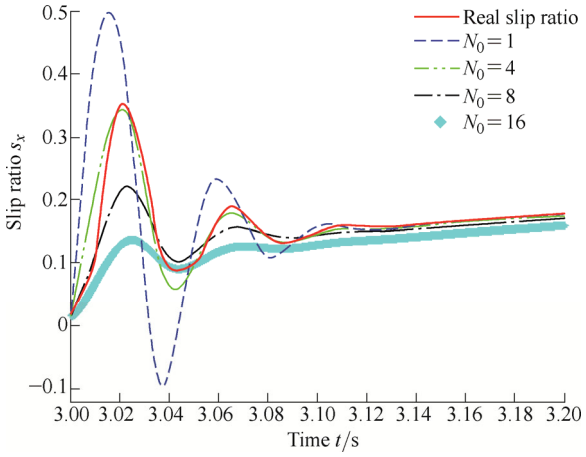

Fig. 9. FFT analysis of slip ratio estimation with various system NFs

To sum up, error in the ESR focuses within a definite frequency zone which is related to the NF of the driving wheel. The LPF proposed in this paper can be used to eliminate the error whose cut-off frequency is decided by the NF of the driving wheel. The filtered ESR converges to the RSR more promptly than original ESR does.

4 Parameters Sensitivity Analysis

In this section, the driving wheel parameters sensitivity

analysis is presented to verify the performance of LPF with appropriated cut-off frequency(N_0=4) based on the above analysis.

The simulation condition doesn't change while K_r, C_r and mass distribution(J_{in}, J_{Ring}) change. The simulation results are show in Figs. 10–12, which indicate that the proposed LPF is robust and effective when the parameters of driving wheel vary in wide ranges.

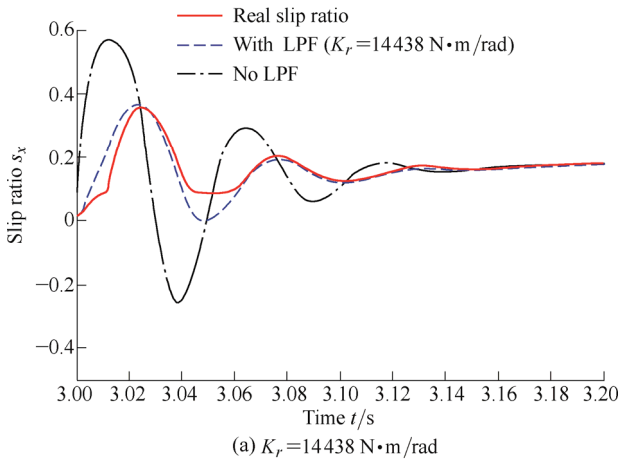

(a) K_r=14438 N·m/rad

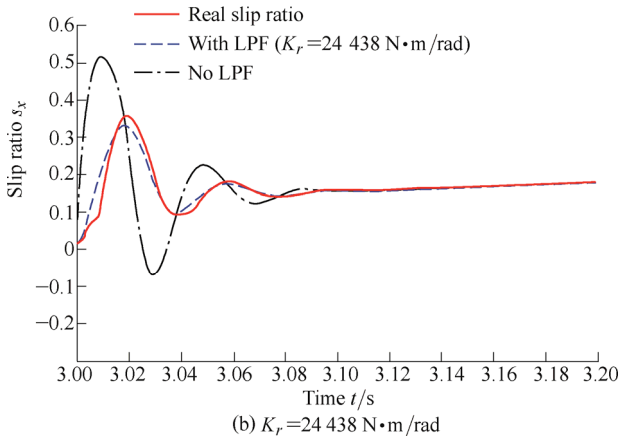

(b) K_r=24 438 N·m/rad

Fig. 10. Slip ratio estimation results with various torsional stiffness values

In a word, the proposed LPF is validated by the simulation results. The parameter sensitivity analysis indicates that the LPF can be used in slip ratio estimation under the vehicle starting and accelerating conditions to eliminate the error caused by tire deformation.

Sensitivity of different road conditions

As the non-linear relaxation model shows, the delay effect in the tire/road interface fades with the SR increase. So the LPF should be verified under different adhesion conditions. The simulation condition remains the same and the adhesion coefficient changes. The simulation results are shown in Fig. 13, which indicates that the LPF(N_0=4) performance is satisfied when adhesion coefficient is between 0.5 and 0.8.

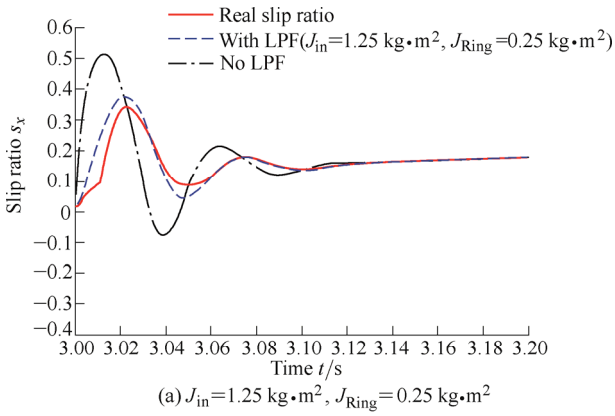

(a) J_{in}=1.25 kg·m^2, J_{Ring}=0.25 kg·m^2

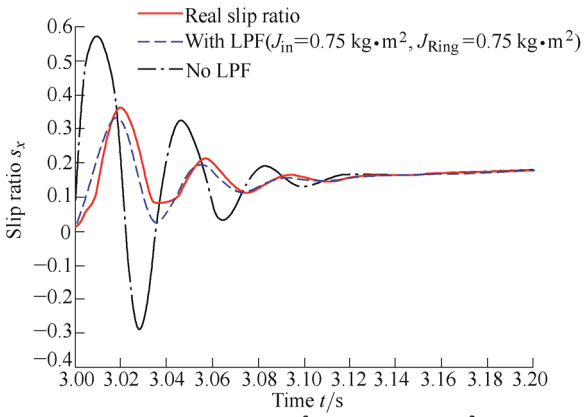

(b) J_{in}=0.75 kg·m^2, J_{Ring}=0.75 kg·m^2

Fig. 11. Slip ratio estimation with various mass distributions

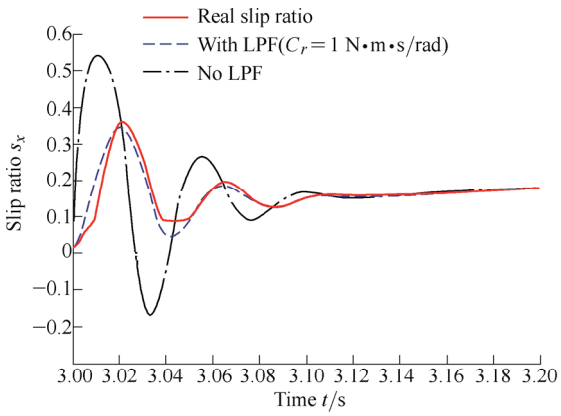

(a) C_r=1 N·m·s/rad

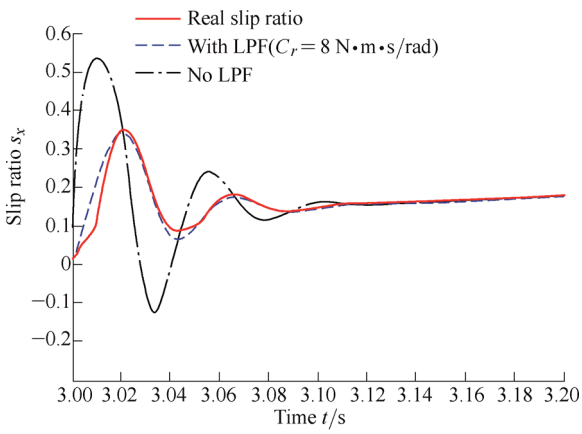

(b) C_r=8 N·m·s/rad

Fig. 12. Slip ratio estimation with various damping coefficient values

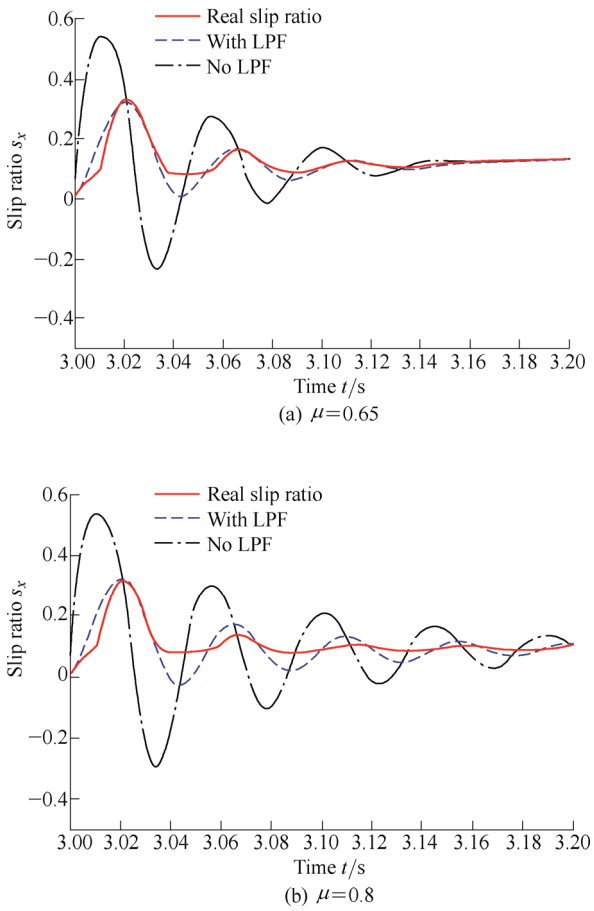

Fig. 13. Slip ratio estimation with different adhesion coefficients

In theory, the LPF should be changed at higher vehicle speed according to the non-linear relaxation model. The modified LPF compensated with the rotor speed is governed by Eq. (28):

$$\begin{cases} f_{\text{cut}} = \dfrac{f_n}{N_0}, & V < 1, \\ f_{\text{cut}} = \dfrac{k\dot{\theta}_{\text{in}} f_n}{N_0}, & V \geqslant 1, \end{cases} \tag{28}$$

where k is a definite constant. However, the error in ESR is not obvious under steady condition as Fig. 14 shows. The steady condition means that the vehicle runs at a constant speed and the tire deformation is constant. Thus the rotary speed of the tire ring and the rotor are equal. As a result, the rotor speed can be used to accurately estimate the SR, and the LPF is not obligatory. Moreover, the motor torque output tends to be saturated when the vehicle speed is high because a large torque is needed to overcome the driving resistance. The torque component used to accelerate the wheel and the vehicle therefore decreases. Hence the rotary speed difference between the rotor and the tire ring inherently decreases.

In a word, the LPF is aimed at solving the slip ratio estimation problem under fierce acceleration/deceleration conditions especially at the low speed region.

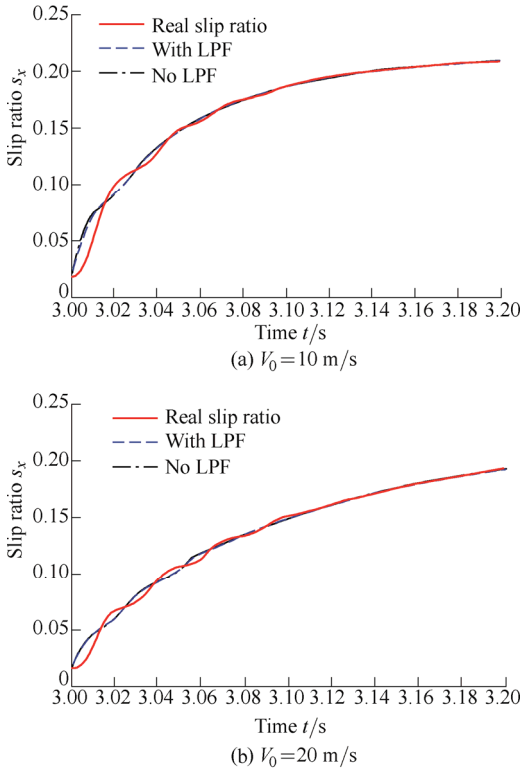

Fig. 14. Slip ratio estimation results at steady conditions when the vehicle speed is high

5 Conclusions

(1) A deformable driving wheel model is proposed to analyze the influence of tire dynamics on the slip ratio estimation. The error in the ESR caused by the difference between the rotor/hub and the ring rotary speeds under the starting/accelerating condition is presented both in the time and frequency domains.

(2) The relationship between the driving wheel NF and the error in ESR are analyzed. The error focuses within a definite frequency zone which is also proportional to the NF. Furthermore, the frequency zone only depends on the NF and has no relation with any other single parameter of the driving wheel.

(3) The LPF is proposed to make ESR converge more promptly to the RSR. Based on the FFT analysis results, the appropriate cut-off frequency of the LPF is obtained. The filtered ESR converges to the RSR fast and the performance is satisfactory.

(4) The proposed LPF is verified by the parameters sensitivity analysis. The robustness of the LPF is verified when several driving wheel parameters, including the K_r, C_r, J_{in}, J_{Ring}, and road adhesion coefficient change in wide ranges.

References

[1] KHALIGH A, LI Zhihao. Battery, ultracapacitor, fuel cell, and hybrid energy storage systems for electric, hybrid electric, fuel cell, and plug-in hybrid electric vehicles: state of the art[J]. *IEEE Transactions on Vehicular Technology*, 2010, 59(6): 2806–2814.

[2] HORI Y. Future vehicle driven by electricity and control-research on four-wheel-motored "UOT Electric March II"[J]. *IEEE Transaction on Industrial Electronics*, 2004, 51(5): 954–962.

[3] MAEDA K, FUJIMOTO H, HORI Y. Four-wheel driving-force distribution method based on driving stiffness and slip ratio estimation for electric vehicle with in-wheel motors[C]//*IEEE Vehicle Power and Propulsion Conference (VPPC)*, Seoul, Korea, October 9–12, 2012: 1286–1291.

[4] HONDA Y, NAKAMURA T, HIGAKI T, et al. Motor design considerations and test results of an interior permanent magnet synchronous motor for electric vehicle[C]//*Proceedings of the IEEE 32nd International Annual Meeting*, New Orleans, USA, October 5–9, 1997: 75–82.

[5] SIMANEK J, NOVAK J, CERNY O, et al. FOC and flux weakening for traction drive with permanent magnet synchronous motor[C]//*Proceedings of the IEEE International Symposium on Industrial Electronics*, Cambridge, UK, June 30–July 2, 2008: 753–758.

[6] BENCHAIB A, POULLAIN S, THOMAS J L, et al. Discrete-time field-oriented control for SM-PMSM including voltage and current constraints[C]//*Proceedings of the IEEE International Conference on Electrical Machines and Drives*, Madison, USA, June 1–4, 2003: 999–1005.

[7] LIN F J, LIN C H. A permanent-magnet synchronous motor servo drive using self-constructing fuzzy neural network controller[J]. *IEEE Transactions on Energy Conversion*, 2004, 19(1): 66–72.

[8] RASMUSSEN H, VADSTRUP P, BORSTING H. Sensorless field oriented control of a PM motor including zero speed[C]//*Proceedings of the IEEE International Conference on Electric Machines and Drives*, Madison, USA, June 1–4, 2003: 1224–1228.

[9] LEE B-R R, SIN K H. Slip-ratio control of ABS using sliding mode control[C]//*The 4th Korea-Russia International Symposium on Science and Technology*, Ulsan, Korea, June 27–July 1, 2000(3): 72–77.

[10] JALALI K, UCHIDA T, MCPHEE J, et al. Development of a fuzzy slip control system for electric vehicles with in-wheel motors[J]. *SAE International Journal of Alternative Powertrains*, 2012, 1(1): 46–64.

[11] FOITO D, GUERREIRO M, CORDEIRO A. Anti-slip wheel controller drive for EV using speed and torque observers[C]//*18th International Conference on Electrical Machines*, Vilamoura, Portugal, September 6–9, 2008: 1–5.

[12] XU Kun, XU Guoqing, LI Weixin, et al. Anti-skid for electric vehicles based on sliding mode control with novel structure[C]//*IEEE International Conference on Information and Automation*, Shenzhen, China, June 6–8, 2011: 650–655.

[13] FUJIMOTO H, FUJII K, TAKAHASHI N. Vehicle stability control of electric vehicle with slip-ratio and cornering stiffness estimation[C]//*IEEE/ASME International Conference on Advanced Intelligent Mechatronics*, Zurich, Switzerland, September 4–7, 2007: 1–6.

[14] SUZUKI T, FUJIMOTO H. Slip ratio estimation and regenerative brake control without detection of vehicle velocity and acceleration for electric vehicle at urgent brake-turning[C]//*IEEE 11th International Workshop on Advanced Motion Control*, Nagaoka, Japan, March 21–24, 2010: 273–278.

[15] PAUWELUSSEN J P, GOOTJES L, SCHRODER C, et al. Full vehicle ABS braking using the SWIFT rigid ring tyre model[J]. *Control Engineering Practice*, 2003, 11(2): 199–207.

[16] ADCOX J, AYALEW B, RHYNE T, et al. Interaction of anti-lock braking systems with tire torsional dynamics[C]//*Meeting of the Tire Society*, Akron, USA, September 13–14, 2011: 1–18.

[17] MASTANDREA M, VANGI D. Influence of braking force in low-speed vehicle collisions[J]. *Proc IMechE Part D: Journal of Automobile Engineering*, 2005, 219(2): 151–164.

[18] VELENIS E, TSIOTRAS P, CANUDAS-DE-WIT C, et al. Dynamics tire friction models for combined longitudinal and lateral vehicle motion[J]. *Vehicle System Dynamics*, 2005, 43(1): 3–29.

[19] CANUDAS-DE-WIT C, TSIOTRAS P, VELENIS E, et al. Dynamic friction models for road/tire longitudinal interaction[J]. *Vehicle System Dynamics*, 2003, 39(3): 189–226.

[20] RILL G. First order tire dynamics[C]//Proceedings of the 3rd European Conference on Computational Mechanics Solids, Structures and Coupled Problems in Engineering, Lisbon, Portugal, June 5–8, 2006: 1–9.

[21] PACEJKA H B. *Tyre and vehicle dynamics*[M]. Oxford: Butterworth-Heinemann, 2002.

[22] BIAN Yongming, ZHU Lijing, LAN Hao, et al. Regenerative braking strategy for motor hoist by ultracapacitor[J]. *Chinese Journal of Mechanical Engineering*, 2012, 25(2): 377–384.

[23] GU Jing, OUYANG Minggao, LI Jianqiu, et al. Driving and braking control of PM synchronous motor based on low-resolution hall sensor for battery electric vehicle[J]. *Chinese Journal of Mechanical Engineering*, 2013, 26(1): 1–10.

[24] SONG Ziyou, LI Jianqiu, OUYANG Minggao, et al. Sensorless control of PMSM with compensated sliding mode[C]//*2012 International Conference on Measurement, Instrumentation and Automation*, Guangzhou, China, September 15–16, 2012: 1226–1233.

[25] SONG Ziyou, LI Jianqiu, OUYANG Minggao, et al. Rule-based fault diagnosis of hall sensors and fault-tolerant control of PMSM[J]. *Chinese Journal of Mechanical Engineering*, 2013, 26(4): 813–822.

Biographical notes

LI Jianqiu, born in 1972, is currently a professor at *Department of Automotive Engineering*, *Tsinghua University*, *China*. He received his PhD degree in power mechanism and engineering from *Tsinghua University*, *China*, in 2000. His research interests include electronic control of diesel engine, key technology of automotive electronics, fuel cell and powertrain control.
Tel: +86-10-6278-5706; E-mail: lijianqiu@tsinghua.edu.cn

SONG Ziyou, born in 1989, is currently a PhD candidate at *State Key Laboratory of Automotive Safety and Energy, Tsinghua University*, *China*. He received his bachelor degree in automotive engineering from *Tsinghua University*, *China*, in 2011. His research interests include in-wheel PMSM control, hybrid energy storage system control, and the EV powertrain optimization.
E-mail: ziyou.song@qq.com

WEI Yintao, born in 1971, is currently a professor at *State Key Laboratory of Automotive Safety and Energy, Tsinghua University, China*. He received his PhD degree in engineering mechanics from *Harbin Institute of Technology, China*, in 1997. His research interests include tire dynamic modeling and control.
E-mail: weiyt@tsinghua.edu.cn

OUYANG Minggao, born in 1958, is currently a professor at *Department of Automotive Engineering, Tsinghua University, China*. He received his PhD degree in mechanical engineering from the *Technical University of Denmark, Lyngby, Denmark*, in 1993. His research interests include new energy vehicles, automotive powertrains, engine control systems, and transportation energy strategy and policy.
E-mail: ouymg@tsinghua.edu.cn